Materials Today: Proceedings 54 (2022) 50–56

Contents lists available at ScienceDirect

Materials Today: Proceedings

journal homepage: www.elsevier.com/locate/matpr

Nanocellulose enriched mortars: Evaluation of nanocellulose properties affecting microstructure, strength and development of mixing protocols

E.G. Deze [a,*], E. Cuenca [b], A.M.L. Násner [c], M. Iakovlev [a], S. Sideri [a], A. Sapalidis [d], R.P. Borg [c], L. Ferrara [b]

[a] API Europe, Karvela 5 Str, 15342 Aghia Paraskevi, Athens, Greece
[b] Department of Civil & Environmental Engineering, Politecnico di Milano, Piazza Leonardo da Vinci 32, Milan 20133, Italy
[c] Faculty for the Built Environment, University of Malta, Msida MSD 2080, Malta
[d] Institute of Nanoscience & Nanotechnology, NCSR "Demokritos" Patr. Gregoriou E & 27 Neapoleos Str, 153 41 Agia Paraskevi, Athens, Greece

ARTICLE INFO

Article history:
Received 27 October 2020
Received in revised form 3 August 2021
Accepted 28 September 2021
Available online 7 November 2021

Keywords:
Cellulose Nanocrystals (CNCs)
Cellulose Nanofibrils (CNFs)
Mortars

ABSTRACT

In this work, four different nanocellulose (NCs) aqueous suspensions (two Cellulose Nano-Fibrils-CNF and a pair of Cellulose Nano-Crystals-CNC) were selected for the evaluation of key aspects that potentially affect the final performance of mortars. The main objective was the development of appropriate mixing protocols that will allow the incorporation of cellulose nanoadditives into cementitious blends. Inclusion of two different NC species into mortars will provide a side-by-side performance comparison between CNCs and CNFs leading to a better understanding of particle morphology impact on the properties of cementitious composites. Moreover, preliminary structural and physicochemical NC characterization tests were performed to enlighten the effects of NC intrinsic features on the final efficiency of the materials. Strength tests of as-obtained NC enriched specimens revealed an enhanced performance when compared to respective reference samples. In particular the presence of CNFs – and specifically AVAP® CNFs– in the mortar mixture resulted in an increase up to 43% in flexural strength values, whereas CNCs were more effective in raising compressive strength values (up to 21%). Supposing that this improvement, emanates from evolving interactions between NCs and defects existing in the matrix at the onset of their formation a more detailed study is on-going aiming at the in depth comprehension of all synoptic parameters that will enable a straight correlation between mortars and nanocellulose properties and will facilitate the use of NCs to upgrade cementitious materials into tailored made composites.

Selection and peer-review under responsibility of the scientific committee of the International Conferences & Exhibition on Nanotechnologies, Organic Electronics & Nanomedicine – NANOTEXNOLOGY 2020.

1. Introduction

Cementitious composites are generally preferred due to their high compressive strength, low-cost preparation, simple production process and convenience of use. However, these composites have many disadvantages such as low tensile capacity and high cracking tendency which affect the long-term durability of structures. In addition, in harsh environments they typically suffer from physical and chemical damage leading to degradation and service life shortening. The introduction of nanomaterials into construction sector, permits the nano and microstructure engineering of mortars and consequently, on the macroscopic behaviour side, tailored and multifunctional composites can be produced with remarkable mechanical performance and durability [1,2]. In this regard, major research areas in the modification of mortars with nanoadditives have so far covered silica [3], titanium dioxide [4,5], nanoclays [6], carbon nanotubes [7] and carbon nanofibers [1]. However, in view of the worldwide policy for facing environmental changes, today's concrete technology moves towards the development and optimization of eco-efficient construction materials utilizing sustainable components with low environmental impact, driving scientific interest to utilization of cellulose nanostructures (NCs) as concrete reinforcing agents [8–10]. These novel materials are promising candidates, being able to combine both the intrinsic cellulose properties, including high strength, high stiffness and low weight with the unique features of nanomaterials (i.e. high reactivity, low surface to volume ratio) [9,10].

* Corresponding author.
E-mail address: enteze@api-europe.gr (E.G. Deze).

https://doi.org/10.1016/j.matpr.2021.09.511
2214-7853/
Selection and peer-review under responsibility of the scientific committee of the International Conferences & Exhibition on Nanotechnologies, Organic Electronics & Nanomedicine – NANOTEXNOLOGY 2020.

Indeed, several research studies claim a significant enhancement in the mechanical properties of concretes with the addition of a modest NCs amount [11,12]. For instance, Cao et al. reported 30% increase in flexural strength of cellulose nanocrystals (CNCs) enriched cement paste attributed to the development of mechanisms that accelerate hydration reactions [13]. A moderate increase in compressive strength was also recorded, which was attributed to the high crystallinity index of CNC (usually accompanied with high Young modulus) and to "filling ability" that enables the elimination of randomly developed small size pores during hydration [12–16]. Incorporation of cellulose nanofibrils (CNFs) into cement pastes was also shown to positively affect the mechanical performance of mortars [10,14,17–19]. Specifically, the hydrophilic nature and highly reactive surface of cellulose nanofibrils allow them to act as nucleation sites facilitating hydration of cement during early age stages [19,20]. As a result, a large volume of products is precipitated and accumulated in the open pores initially filled with water, leading to the formation of a more homogenous and compact microstructure [10,14,18–20]. Additionally, their high water adsorption capacity allows them to operate as water reservoirs that gradually release water to the matrix in dry environments, enabling continuing hydration which contributes to further pore refinement and -in case- to microcrack sealing [9]. Likewise, owing to their high aspect ratio they arrest microcrack propagation and improve the stress transfer at matrix- fibrils interface ("bridging effect") [9,17,18,20].

Overall, there is a great potential in the use of NCs (CNCs or CNFs) as reinforcing agents for cementitious composites, which in a long term perspective, could also enhance work efficiency, shortening intermediate curing times and subsequently reducing operational costs [9,14,17,20]. Within this context, the current study - performed under the scope of H2020 ReSHEALience project (GA760824)-, has the intention of taking the advantage of the nanocellulose to upgrade the current High Performance Concrete technology to Ultra High Durability Concrete (UHDC) and applying them in two European pilot demonstration facilities. To this end, the produced specimens contained crystalline admixtures, steel fibers as well as cellulose nanocrystals (CNCs) or cellulose nanofibrils (CNFs) from two sources. Incorporation of different NC species into cementitious mixtures will offer a comparative performance between CNCs and CNFs leading to a better understanding of particle morphology impact on the composite properties. Comprehensive analysis of both structural and physicochemical characteristics of NC additives that may potentially affect the material performance has been performed with the aim of providing a straight correlation between concrete efficiency and nanocellulose inherent properties, in view of meeting manufacturer requirements in terms of proper selection of NC species, additive content and fresh cement paste rheology.

2. Materials and methods

2.1. Materials

Four nanocellulose-enriched High-Performance Fiber Reinforced Cementitious Composites (HPFRCCs) were casted from Politecnico di Milano (PoliMi) and University of Malta (UoM) research groups. The composition of mixtures is illustrated in Tables 1 and 2, respectively.

A HPFRCC mixture containing CEM I 52.5 and slag as binders, sand, crystalline admixtures and steel fibers was used as reference material in the case of PoliMi. In the same context, a mixture containing CEM 52.5 and silica fume as binders, sand, crystalline admixtures and steel fibers was casted by UoM. While the use of slag, silica fume is quite common, it is worth remarking here that crystalline admixtures were used as self-healing stimulators, targeting a new concept of ultra-high durability materials. The adopted mixing procedures and the employed dosages of constituents were formulated to guarantee self-compacting properties. In all cases, the water-to-cement ratio remained constant and equal to 0.33 (with a total water/binder ratio equal to about 0.18).

Table 1
Mix composition of investigated mortars casted by PoliMi.

Constituents (kg/m^3)	Reference	AVAP® CNCs-Reference	AVAP® CNFs-Reference
CEM I 52.5R	600	600	600
Slag	500	500	500
Water	200	200	200
Steel Fibers (l_f = 20 mm; d_f = 0.22 mm) (Azichem Readymesh 200®)	120	120	120
Sand 0–2 mm	982	982	982
Superplasticizer (Glenium ACE 300®)	33	33	33
Crystalline admixtures (Penetron Admix®)	4.8	4.8	4.8
AVAP® CNCs[1]	–	0.15	–
AVAP® CNFs[1]	–	-	0.15

[1] % by weight of cement.

Table 2
Mix composition of investigated mortars casted by UoM.

Constituents (kg/m^3)	Reference	Navitas CNCs-Reference	UMaine CNFs-Reference
CEM 52.5	700	700	700
Silica Fume	400	400	400
Water	231	231	231
Superplasticizer (Glenium ACE 442®)	64	64	64
Sand 117/F	286	286	286
Sand 103	409	409	409
Sand 113	122	122	122
Steel Fibers (l_f = 20 mm; d_f = 0.22 mm)	160	160	160
Crystalline admixtures (Penetron Admix®)	5.6	5.6	5.6
Navitas CNCs[1]	–	0.15	–
UMaine CNFs[1]	–	-	0.15

Following the same experimental protocols two additional mixtures were produced in each group containing also cellulose nanocrystals (CNCs) and cellulose nanofibrils (CNFs) (Tables 1, 2). Two of the nanocellulose components were produced through the patented AVAP® biorefinery technology and utilized by PoliMi, whereas the other two were obtained from University of Maine and Navitas Company respectively and casted using UoM mixing protocol. Prior to their addition to cements, all nanocellulose additions were dispersed in water at a loading of 1.5%wt, that was further decreased by an order of magnitude when mixed with the rest of composite components. In an attempt to avoid workability issues faced during the addition of UMaine CNFs into the blend, superplasticizer and water pH adjusted to the basic region were investigated as nanocellulose dispersion media. Application of high shear rates was also performed to assist homogeneity of suspension. The main target was to break the formed aggregates and charged particles surface so that polymeric components could repel each other and remain in a dispersed state. Amongst the two media, pH adjusted aqueous media provided better results and was therefore selected for the preparation of specimens. After mixing, materials were casted in appropriate molds to produce

prismatic 40 × 40 × 160 mm beam specimens for flexural and compressive strength tests.

2.2. Samples characterization

FT-IR measurements were conducted using a Thermo scientific Nicolet 6700 FT-IR spectrometer equipped with attenuated total reflection diamond crystal – ATR, CO_2 and moisture removal system and Mercuric Cadmium Telluride- MCT wide spectrum detector cooled with liquid nitrogen. The instrument provided the ability to place the gridded polymeric samples directly on a diamond surface (ATR method). The spectra were recorded in the range 4000–400 cm^{-1} at 4 cm^{-1} resolution and 64 scans per spectrum in the transmission mode. For X-ray diffraction measurements, polymeric gels were placed on microscope glass slides and allowed to dry in a silica desiccator for 72 h. The patterns were acquired using a Rigaku rotating anode X-ray generator (operating at 50 kV, 100 mA, nickel filtered CuKa1 radiation) and a R-A[1]XIS IV imaging plate. Scan parameters were set at 2 s per step with 0.05° step resolution in the range of 2θ. The thermal stability of nanoadditives was analyzed using a SETARAM SETSYS Evolution 18 thermogravimetric analyzer. All samples were heated from 50 to 600 °C at a heating rate of 10 °C/min under argon flow (40 ml/min). Viscosity properties of each sample were assessed using a V1-L/ V2-L viscometer equipped with special spindle adapter for low viscosity materials (LCP). Prior to each experiment, viscometer zero gap was set through calibration and measurements were performed with approximately 20 ml of polymeric aqueous suspensions of known concentrations that were carefully loaded on the center of the lower viscometer plate. The sets of experiments were repeated 5 times for each sample. The mechanical performance of as prepared plain and NC enriched specimens was evaluated by flexural toughness (3-point bending) and compressive strength tests. Flexural tests were performed according to EN 1015-11:1999 on prismatic specimens (40 × 40 × 160 mm). For this purpose, a 7 mm deep notch was cut at mid-span of the specimens. Three-point bending tests were performed in displacement control by measuring the Crack Mouth Opening Displacement (CMOD) at the tip of the notch. Then, once each specimen was completely tested in flexure and broken in two halves, compressive strength tests were performed also according to EN 1015-11. Tests were performed after 7 and 28 days curing of the specimens at climate room conditions (T = 20 °C and 95% RH). Morphological investigation of materials was conducted with a Jeol JSM 7401F Field Emission Scanning Electron Microscope equipped with Gentle Beam mode and EDAX analyzer. The applied acceleration voltage was 2 kV and samples were mounted on metallic (brass) substrates using a double coated carbon conductive tape.

3. Results and discussion

3.1. FT-IR analysis

FTIR spectroscopy has been extensively used in cellulose research since it represents a relatively easy method for obtaining direct information on functional groups present on nanocellulose materials. Recorded FT-IR spectra of the examined NC samples and the summary of transmittance signals associated with the corresponding bond vibrations are illustrated in Fig. 1 and Table 3, respectively.

It is evident that little difference is seen between the individual bond vibrations within CNCs and CNFs, other than changes in intensity (Fig. 1). All spectra display the characteristic α-cellulose peaks coherent with those available in the literature [21,22]. In particular, the absorption peaks at ~2893 cm^{-1} and around 1025 cm^{-1} are attributed to C–H and O–H stretching vibrations, respectively. The latter is related to glycosidic $^4C1$ ring conformation deformation and β-glycosidic linkages between glucopyranose rings in cellulose. The band located at 1644 cm^{-1} is reported as O–H vibration of adsorbed water. The peak at 1382 cm^{-1} is attributed to C–H and C–O vibrations in the monosaccharide unit rings of cellulose. On the other hand, the vibration of C–O–C in pyranose ring is indicated by the absorption peak at 1060 cm^{-1} [23,24]. Finally, the band shown at ~1430 cm^{-1} is associated with the crystalline regions within cellulose, whereas the peak at ~895 cm^{-1} is generally assigned to the amorphous regions of cellulose. It is worth mentioning that characteristic bands attributed to carboxylic (~1729 cm^{-1}) and sulphate (~1376 cm^{-1}) functional groups or lignin compounds (~3570 cm^{-1}, ~1715–1675 cm^{-1}, ~1602–1502 cm^{-1}) could not be distinguished in all spectra, signifying the absence of these groups in NC polymeric chains [21,23,25]. It is well documented that the presence of lignin residual components in nanocellulose structures improves polymer hydrophobicity, making them more compatible with non-polar systems and therefore complicating additive integration into cementitious mixture. Accordingly, the presence of carboxylic or sulfate functional groups promotes the formation of an extensive network of inter molecular hydrogen bonds that may negatively affect solidification process, transfusing brittleness to cementitious matrix.

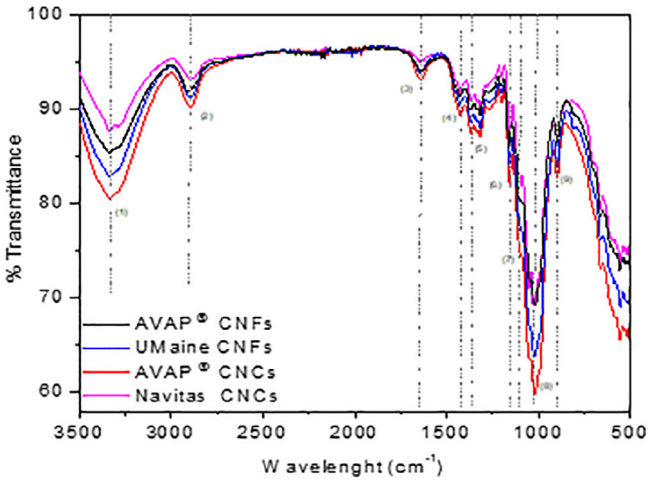

Fig. 1. FTIR spectrums of NC fibrils (CNFs) and crystals (CNCs).

Table 3
Infrared band assignments for NC additives.

Wavenumber range (cm^{-1})	Characteristic bands
(1) 3500–3200	OH stretching
(2) 3000–2835	Aliphatic C–H stretching
(3) 1652–1623	OH bending (absorbed water)
(4) 1470–1420	C–H symmetric bending (CH_2)
(5) 1391–1368	C–H & C–O pyranose ring bending
(6) 1260–1150	C–O–C stretching
(7) 1100–1056	Out of base bending
(8) 1046–994	C–C, C–OH, C–H pyranose ring & side groups
(9) 900–890	C–O–C, C–C–O, C–C–H deformation & stretching

3.2. X-ray diffraction

X-ray diffraction was used to characterize the crystal structure of nanocellulose materials. The corresponding diffractograms are shown in Fig. 2.

[1] by % wt of cement

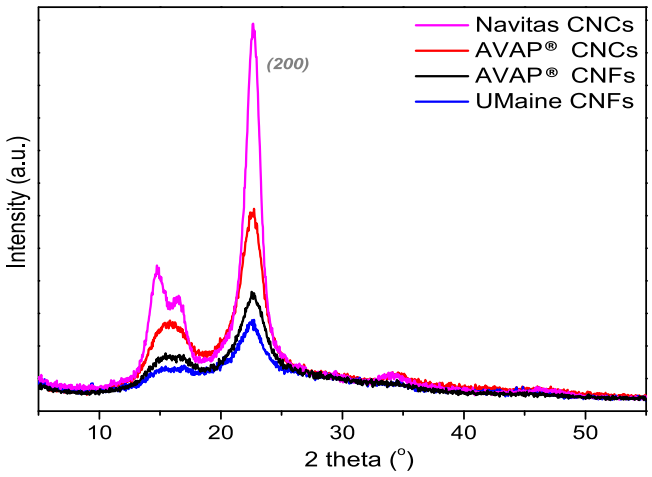

Fig. 2. XRD patterns of NC fibrils (CNFs) and crystals (CNCs).

Two main diffraction peaks are illustrated in most NC materials. The first broad one occurs at around 15.7° which correspond to overlap of peaks assigned to (110) and (110−) respectively, whereas the higher order Bragg reflection centered at 22.6° is a characteristic reflection of (200) crystalline peak. These polymorphs correspond to the cellulose I structure, characterized with a parallel arrangement of two anydroglucose chains and has been referred to as the polymorph of cellulose with the highest mechanical integrity [26,27]. In the case of Navitas CNCs, the center positions of crystalline peaks in low angle area as determined from the XRD profile are at 14.6° and 16.4° in the form of a bimodal peak with higher intensity.

The average crystallite sizes calculated from the fitted Gaussian (200) reflection peaks using the Scherrer formula (shape factor 0.9) are compiled in Table 4. The (200) diffraction peaks were fitted to the profiles after subtracting the linear background without assuming the presence of non-crystalline scattering usually centered at around 20.6°. The results demonstrate that the average crystal sizes range between 3.4 nm and 3.7 nm, except from Navitas CNCs material in which crystal size amounts to 6 nm.

For additional reasons, the crystallinity index (CI) of examined polymeric nanostructures was also derived. The calculations were accomplished using the empirical Segal equation (1), by measuring peak intensities of crystalline (I_{002}) and amorphous regions (I_{am}) having subtracted baseline [25]:

$$CI(\%) = \frac{I_{002} - I_{am}}{I_{002}} x100\% \quad (1)$$

In the current study, the reflection at 22.6° was used for I_{002} and the one centered at 15.7° for the estimation of I_{am} region. The peak shown at 14.6° in Navitas CNCs pattern was used for calculating I_{am}, as well. The derived crystallinity values are summarized in Table 4. In accordance with crystal sizes obtained from Scherrer formula, also in this case Navitas CNCs possesses the highest crystallinity index reaching a value of 79%, followed by AVAP® CNCs with 58%. As expected, this percentage is further decreased down to 52% in the case of nanofibrillated materials signifying the presence of a higher amorphous cellulose fraction as well as residual hemicelluloses in these samples.

3.3. Thermal stability

The thermal stability of nanocellulose samples was assessed through TGA/DSC measurements. It has been well established, that this inherent characteristic greatly depends on the presence of sulfate or phosphate groups on polymeric chains, which serve as catalysts in dehydration of pyranose ring and materials degradation [10,23]. The corresponding TGA/DTG profiles along with DSC curves are illustrated in Fig. 3.

Table 4
Crystal size & crystallinity index of nanocellulose materials.

Sample	Crystal Size (nm)	Crystallinity Index (%)
Navitas CNC	6	79.07
AVAP® CNC	3.77	58.11
AVAP® CNF	3.32	51.43
UMaine CNF	3.41	52.54

As seen, all samples exhibit analogous thermal degradation patterns demonstrating an initial weight loss at around 70 °C related to the desorption of physically adsorbed water and volatile compounds (Fig. 3, top). Likewise, the major steep weight loss evident in the range 245–350 °C can be assigned to onset and maximum rate of crystal decomposition, accompanied by the complete removal of the organic content at higher temperatures. All degradation reactions are completed at approximately 380 °C. Furthermore, TGA curves of cellulose nanocrystals are slightly shifted towards higher temperatures, signifying a moderately delayed onset of decomposition temperature when compared to those of nanofibrils. The latter could be attributed to the higher crystallinity index of CNCs, as derived from XRD analysis. On the contrary, the higher percentage of amorphous cellulose present in CNF samples, along with their high specific surface area and the large number of free-end chains, promote a greater exposure to heat and partial disruption of cellulose crystal structure that assist thermal degradation reactions [28–30]. Moreover, hemicelluloses in CNF with the irregular structure and low molecular weight are known to be less thermally stable compared to cellulose. These results are further validated from dTG curves, in which crystal decomposition is observed at 328 ± 5 °C for CNC materials, shifting towards lower temperatures (300 ± 5 °C) in the case of nanofibrils. A consequent behavior is also observed for the final mass residue which increases from about 28 to 35% for CNCs and CNFs, respectively, which is attributed to the presence of impurities that greatly enhance char formation [31].

Differential scanning calorimetry (DSC) was also performed in order to elucidate the onset of melting and crystallization temperature (Fig. 3, bottom). In accordance with TGA/dTG results, similar patterns appear also in the DSC thermograms demonstrating a sharp and well-defined exothermic peak at 300 °C and 328 °C for CNFs and CNCs respectively, assigned to crystal decomposition phenomena. A slight decrease of about 20 °C in the onset of decomposition temperature is also observed in Navitas CNCs when compared to the other samples. Nonetheless, that sample exhibits the highest degradation enthalpy attributed to its increased crystallinity degree and inner hydrogen bonding, resulting in a more stable structure [32]. The second lower intensity peak appearing only in CNCs curves at higher temperatures is also assigned to crystal fusion phenomena.

3.4. Viscosity

The rheological properties of nanocellulose aqueous suspensions may have important consequences during their processing and combination with other components. These properties are often profoundly affected by the hydrodynamic shear during flow, pumping and mixing that consequently influence manufacturing operations. In an attempt to ensure good workability of nanocellulose enriched mixtures while maintaining a sufficient polymer amount in the final composite, the rheology of as-examined nanocellulose aqueous suspensions was investigated.

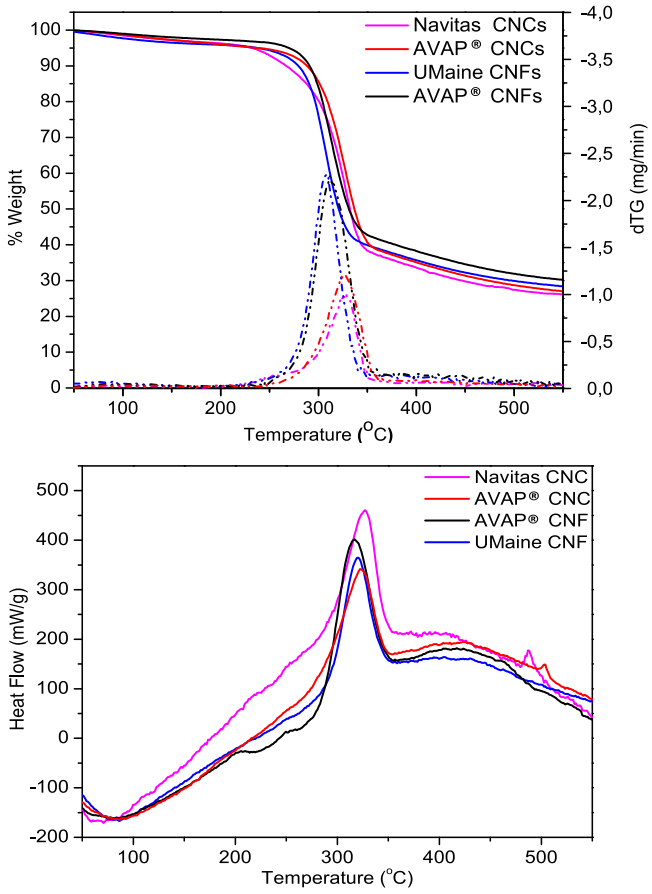

Fig. 3. TGA/DTG (top) and DSC (bottom) thermograms of NC fibrils (CNFs) and crystals (CNCs).

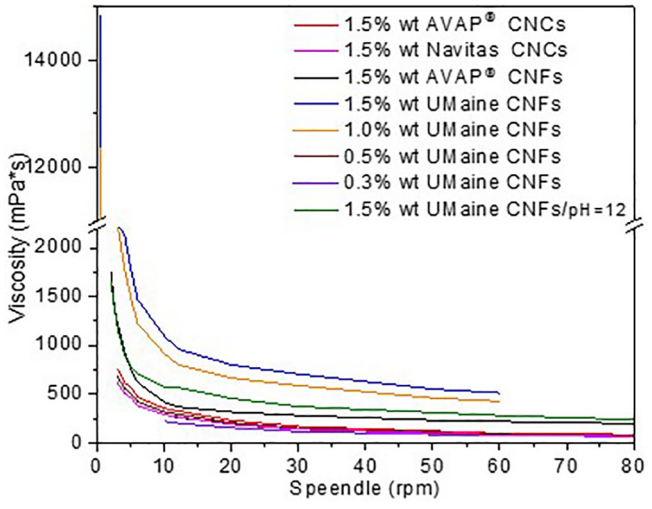

Fig. 4. Viscosity of NC suspensions at different concentrations.

The initial target loading was set equal to the one selected for polymers predilution step (1.5%wt). As seen in Fig. 4, all polymers exhibit a thixotropic, shear thinning (pseudoplastic) behavior demonstrating gradually lower viscosity values at higher shear rates. Nanostructures are colloidal at lower shear rates, and as the rate increases, polymeric chains disentangle until they are fully separate and their axis is parallel to the direction of flow. Among all the samples, the two CNC materials demonstrate lower viscosity values ranging between 600 and 750 mPa*s at low shear rates (~2.5 rpm) indicating the presence of weak particle–particle interactions which in turn provide a better flowability during the mixing process. Over the entire range of studied shear rates, cellulose nanofibril suspensions are more viscous with UMaine CNFs possessing the highest values (up to 15,000 mPa*s). In general, some of the factors that can strongly influence rheology of a suspension include the morphology (particle size, size distribution and shape), the number of particles and the volume fraction they occupy, the surface area, inter and intraparticle interactions and the surface charge. All these parameters are already scheduled to be further investigated in order to shed light and help understanding the developed interactions between polymeric networks and cementitious components that may potentially influence materials final properties.

In an effort to obtain a suspension with similar viscosity to that of the other samples, several UMaine CNF dilutions of lower concentrations were prepared and examined for their viscosity (Fig. 4). It is observed that with reducing the concentration by 1/3, the viscosity is only slightly affected, whereas the desired flow properties are achieved with CNF loading equal to 0.5%wt or 0.3% wt. It is noted that these concentrations refer to nanocellulose loading during the predilution step that will be further reduced by an order of magnitude when mixed with the rest of concrete constituents. In view of the insufficient effect of polymer addition on mortar final properties and the increased amount of water that will be utilized during predilution step and drastically reduce the amount available for mixing the rest of the ingredients, it was decided to slightly modify the pH of UMaine CNFs suspension media to a value comparable to that already prevailing in cement pastes. As demonstrated, the flowability of as prepared 1.5%wt UMaine CNFs suspension at pH ~12 has been considerably improved leading to its selection for the preparation of specimens.

3.5. Mechanical properties & morphological characterization of nanocellulose containing mortars

Tables 5 and 6 summarize the results of flexural and compressive strength tests of as developed NC enriched specimens cured under moist room conditions. According to the results, the presence of NCs positively affects the performance of specimens, irrespective of the mixture components. One possible reason could be the evolving interactions between NCs and defects existing in the matrix at the very onset of their formation. More specifically, it is well evident that flexural strength values demonstrate a higher improvement, especially when cellulose nanofibrils are present in the matrix. In particular, the addition of AVAP® CNFs results in an increase of up to 43% at 7 days, that is reduced down to 16% after 28 days of curing. On the other hand, strength enhancement of the specimen containing UMaine CNFs is lower and remains almost unchanged from 7 to 28 days curing (~16%). In both cases, the efficiency of cementitious materials is similar to those of analogous systems already reported in the literature [8,9,33]. Nonetheless, the performance of specimens holding CNCs in their structures is much lower, as in this case flexural strength values are not being improved more than 8% in both age stages.

Contrarily to what is stated for flexural strength, compressive strength tests demonstrate that CNCs are more effective in increasing material performance, as the corresponding compressive strength values for the Navitas CNCs containing mortar rise up to 21% and 14% at the age of 7 and 28 days, respectively. The analogous trend is also followed by the composites incorporating AVAP® nanocrystals. Since FTIR analysis did not reveal the presence of different functional groups in the samples, the modest improvement in compressive strength could be attributed to CNCs higher crystallinity index, with the crystals inherently supplying their higher

Table 5
Compressive and flexural strength properties of NC containing specimens & reference material casted by PoliMi.

Additive	Flexural Strength (MPa)		Compressive Strength (MPa)	
Reference	7d	15.76	7d	109.2
	28d	24.43	28d	132
AVAP® CNF	7d	27.78	7d	107.3
	28d	29.14	28d	137.7
AVAP® CNC	7d	–	7d	–
	28d	27.35	28d	147.6

Table 6
Compressive and flexural strength properties of NC containing specimens *and reference material casted by UoM.*

Additive	Flexural Strength (MPa)		Compressive Strength (MPa)	
Reference	7d	29.97	7d	83.94
	28d	34.43	28d	135.47
UMaine CNF	7d	35.84	7d	130.78
	28d	39.80	28d	134.86
Navitas CNC	7d	31.11	7d	106.37
	28d	35.09	28d	158.22

strength to the matrix. This is also supported by the XRD and TGA results.

Based on these results, it could be hypothesized that the beneficial role of NC presence in cementitious mixtures can also be rooted in a synergetic effect of NCs particle size and crystalline structure. In particular, cellulose nanofibrils in comparison with the smaller crystals have the right size to divert and accumulate into the matrix defects that are originally filled with water, contributing to the refinement of micro-porosity. Beyond that, the hydrophilic nature of NCs and their tendency to interact with cementitious constituents facilitate hydration reactions and the formation of insoluble products (C-S-H) that also fill the pore network leading to further refinement and matrix solidification [16–19]. Considering also the XRD and TGA analysis results that highlight the presence of a higher amorphous fraction in CNF structures it could be suggested that the enhanced efficiency of CNF enriched specimens, is due to the higher diffusivity of water molecules through the amorphous regions of the nano-constituents. In that way, hydration of cement particles is facilitated at early ages increasing the number of hydration sites and the population of inorganic hydration products.

Morphological characteristics of NC-enriched specimens and reference material were investigated through SEM measurements. Preliminary results of the plain sample and those containing AVAP® nano-additives are illustrated in Figs. 5 and 6, respectively. As seen, all materials demonstrate the typical morphology of cementitious composites. In case of reference sample, regions of different morphologies can be distinguished attributed to the presence of amorphous C-S-H and –to a lesser extent– CaOH hydration products (Fig. 5). Small cracks and pore openings also prevail in the surface of reference sample.

On contrary, SEM pictures of NC containing samples reveal that hydration products exist in a much higher degree justifying the improved strength properties and the enhanced hydration rhythm resulting from the existence of polymeric substitutes in the matrix. Also in these cases, the presence of C-S-H was dominant while a larger population of crystalline CaOH was detected in both samples when compared to reference material. The beneficial role of CNF presence into cementitious mixture with respect to facilitation of hydration reactions and increase of microstructure consistency is well evident in the micrograph of Fig. 6. Here, the nanofibrillated cellulosic component appears to act as nuclei for hydration reactions and as bridge binding inorganic constituents.

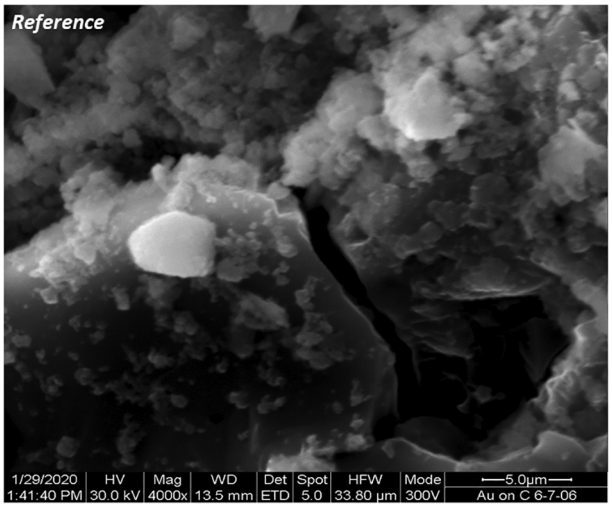

Fig. 5. SEM micrographs of reference specimen cured under moist conditions.

In an attempt to go one step further from preliminarily of results and perceiving the dynamic and complexity of systems such as mortars, further investigation of parameters study is already planned for the near future. Regarding nanocellulose samples, both AFM and SEM analysis will be performed in a complementary manner in order to investigate the morphology, dimensions, aspect ratio and size distribution of materials, whereas DLS technique will provide information related to wet particle size, surface charge and statistical size distribution of active nanocellulose particles. Water adsorption measurements will also be performed in order to evaluate the available H2O sorption sites and reactivity of polymeric nanostructures. Of course, properties of as derived specimens also at later ages, such as porosity, degree of hydration and morphological characteristics will provide valuable information and are expected to shed light onto the observed variations in the performance of NC enriched mortars.

4. Conclusions

This work has been focused on the development of nanocellulose enriched mortars and the evaluation of the effect of NC inher-

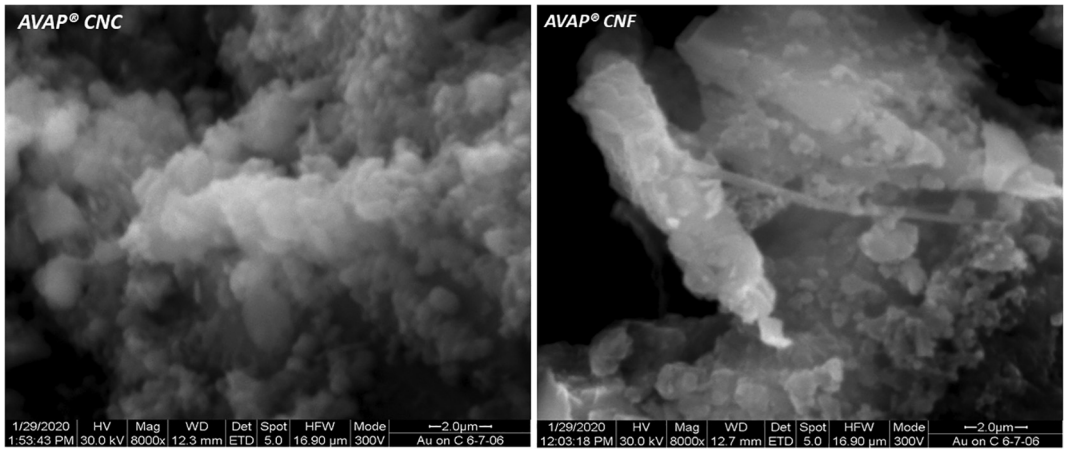

Fig. 6. SEM micrographs of AVAP® enriched specimens cured under moist conditions.

ent properties on the material final performance. To this end four different nanocellulose suspensions (two CNFs and two CNCs) were selected and properly incorporated into cementitious blends at a constant 0.15%wt loading. Flexural strength test results indicated that fracture properties of NC-cementitious composites were improved up to almost 40%, especially when CNFs are present at the mixture. It was suggested that nanocellulose reinforcing ability is a result of a combination between hydration reactions acceleration that increases the number of insoluble products and porosity decrease. CNFs were shown to be more effective likely due to the higher amorphous fraction that facilitates the diffusion of water molecules and the hydration reaction. CNCs contributed more to compressive strength performance due to the higher crystallinity index. Further characterization tests including SEM/AFM, DLS, H_2O diffusion and MIP along with N_2 adsorption/desorption porosimetry will be performed in order to elucidate NCs reinforcement mechanisms with the prospect of providing a straight correlation between the efficiency of nanocellulose enriched cementitious composites and nanocellulose intrinsic properties.

CRediT authorship contribution statement

E.G. Deze: Conceptualization, Methodology, Formal analysis, Writing – original draft. **E. Cuenca:** Conceptualization, Methodology, Formal analysis. **A.M.L. Násner:** Conceptualization, Methodology, Formal analysis. **M. Iakovlev:** . **S. Sideri:** Conceptualization, Resources, Project administration. **A. Sapalidis:** Conceptualization, Methodology, Formal analysis. **R.P. Borg:** Conceptualization, Methodology, Writing – review & editing. **L. Ferrara:** Conceptualization, Methodology, Resources, Writing – review & editing, Supervision, Project administration.

Declaration of Competing Interest

The authors declare that they have no known competing financial interests or personal relationships that could have appeared to influence the work reported in this paper.

Acknowledgements

This research is financed from European Union's Horizon 2020 research and innovation program in the context of ReSHEALience project (Rethinking coastal defence and Green-energy service infrastructures through enhanced-durability high performance cement-based materials) under grant agreement No 760824.

References

[1] F. Sanchez, K. Sobolev, Constr. Build. Mater. 24 (11) (2010) 2060–2071.
[2] H.M. Jennings, J.W. Bullard, J.J. Thomas, J.E. Andrade, J.J. Chen, G.W. Scherer, J. Adv. Concr. Technol. 6 (1) (2008) 5–29.
[3] A.M. Said, M.S. Zeidan, M.T. Bassuoni, Y. Tian, Constr. Build. Mater. 36 (2012) 838–844.
[4] J. Chen, S.C. Kou, C.S. Poon, Cem. Concr. Compos. 34 (5) (2012) 642–649.
[5] D. Osborn, M. Hassan, H. Dylla, Trans. Res. Rec. 2290 (2012) 147–153.
[6] N. Tregger, M. Pakula, S. Shah, Trans. Res. Rec. 2141 (2010) 68–74.
[7] M.S. Konsta-Gdoutos, Z.S. Metaxa, S. Shah, Cem. Concr. Compos. 32 (2010) 110–115.
[8] O.A. Hisseine, W. Wilson, L. Sorelli, B. Tolnai, A. Tagnit-Hamou, Constr. Build. Mater. 206 (2019) 84–96.
[9] L. Jiao, M. Su, L. Chen, Y. Wang, H. Zhu, H. Dai, PLoS One 11 (12) (2016) 1–13.
[10] V. Kokol, M. Bozic, R. Vogrincic, A. Mathew, Carbohydr. Polym. (2015) 1–13.
[11] O. Onuaguluchi, D. Panesal, M. Sain, Cem. Concr. Compos. 68 (2016) 96–108.
[12] T. Fu, F. Montes, P. Suraneni, J. Youngblood, J. Weiss, Polymers 9 (2017) 424.
[13] Y. Cao, P. Zavaterri, J. Youngblood, R. Moon, J. Weiss, Cem. Concr. Compos. 56 (2015) 73–83.
[14] X. Sun, Q. Wu, S. Ren, T. Lei, Springer Science & Business Media (2015).
[15] M. Awais, W. Ahmed, Master thesis, PoliMi (2018/2019), pp. 66-87.
[16] Y. Cao, P. Zavattieri, J. Youngblood, R. Moon, J. Weiss, Constr. Build. Mater. 119 (2016) 71–79.
[17] M. Ardanuy, J. Claramunt, R. Arevalo, F. Pares, E. Aracri, T. Vidal, BioResources 7 (3) (2012) 3883–3894.
[18] R. Mejdoub, H. Hammi, J. Sunol, M. Khitouni, A. Mnif, S. Boufi, J. Compos. Mater. (2016) 1–13.
[19] O. Onuaguluchi, D. Panesal, M. Sain, Constr. Build. Mater. 63 (2014) 119–124.
[20] X. Sun, Q. Wu, S. Lee, Y. Qing, Y. Wu, Nat. Sci. Rep. 6 (2016) 31654.
[21] S. Kyle, Z. M. Jessop, A. Al-Sabah, K. Hawkins, A. Lewis, T. Maffeis, C. Charbonneau, A. Gazze, L. W. Francisc, M. Iakovlev,, Kim Nelson, S. J. Eichhorn, I. S. Whitaker, Carbohydr. Polym. 198 (2018) 270–280.
[22] Y. Chen, H. Lee, J. Juan, S. Phang, Carbohydr. Polym. 151 (2016) 1210–1219.
[23] A. Mandal, D. Chakrabarty, Carbohydr. Polym. 86 (2011) 1291–1299.
[24] J. Li, X. Wei, Q. Wang, J. Chen, G. Chang, L. Kong, J. Su, Y. Liu, Carbohydr. Polym. 90 (2012) 1609–1613.
[25] W. Wulandari, A. Rochliadi, I. Arcana, Mater. Sci. Eng. 107 (2016) 012045.
[26] A.D. French, Cellulose 21 (2014) 885–896.
[27] M. Paakko, M. Ankerfors, H. Kosonen, A. Nykanen, S. Ahola, M. Osterberg, T. Lindstrom, Biomacromolecules 8 (6) (2007) 1934–1941.
[28] M. Sofla, M. Brown, T. Tsuzuki, Adv. Nat. Sci.: Nanosci. Nanotechnol. 7 (3) (2016) 778–815.
[29] G. Paschoal, C. Muller, G. Carvalho, Quimica Nova 38 (4) (2015) 478–482.
[30] P.G. Gan, S.T. Sam, M. Abdullah, M. Omar, J. Appl. Polym. Sci. (2020), https://doi.org/10.1002/APP.48544.
[31] S. Gea, C. Reynolds, N. Roohpour, B. Wirjosentono, N. Soykeabkaew, E. Bilotti, T. Peijs, Bioresour. Technol. 102 (2011) 9105–9110.
[32] S. Huang, L. Zhou, M. Li, Q. Wu, D. Zhou, Materials 10 (2017) 80, https://doi.org/10.3390/ma10010080.
[33] N. Buch, O. Rehman, J. Hiller, J. Transp. Res. Board (1999) 72–80.